Journal of Power Sources 266 (2014) 150–154

Contents lists available at ScienceDirect

Journal of Power Sources

journal homepage: www.elsevier.com/locate/jpowsour

Short communication

Nitrogen-doped $Li_4Ti_5O_{12}$ nanosheets with enhanced lithium storage properties

Baofeng Wang [a,*], Junsheng Wang [a], Jie Cao [a], Honghua Ge [a], Yufeng Tang [b,*]

[a] College of Environmental and Chemical Engineering, Shanghai University of Electric Power, Shanghai 200090 China
[b] CAS Key Laboratory of Materials for Energy Conversion and State Key Laboratory of High Performance Ceramics and Super Fine Microstructure, Shanghai Institute of Ceramics, CAS, Shanghai 200050, China

HIGHLIGHTS

- N-doped $Li_4Ti_5O_{12}$ was prepared by hydrothermal route and following sintering in NH_3.
- N-doped $Li_4Ti_5O_{12}$ has nanosheets structure.
- Synergistic effect of N-doping and nanostructure leads to high rate performance.
- N-doped $Li_4Ti_5O_{12}$ shows improved cycle stability and specific capacity at high rate.

ARTICLE INFO

Article history:
Received 25 February 2014
Received in revised form
5 May 2014
Accepted 5 May 2014
Available online 14 May 2014

Keywords:
Lithium ion batteries
Anode material
Lithium titanate oxide
Doping

ABSTRACT

N-doped $Li_4Ti_5O_{12}$ nanosheets (NLTO) have been prepared by a simple hydrothermal reaction with further heat treatment at low temperature (500 °C) under NH_3 atmosphere. The effects of the Nitrogen on structure and electrochemical performance are extensively studied. XRD results show that nitrogen doping does not change the $Li_4Ti_5O_{12}$ (LTO) crystal structure. TEM and SEM results indicate the as-synthesized NLTO has an irregular nano-sheet-like structure with a size of 50–200 nm, which results in short Li^+ diffusion paths and rapid charge transfer reactions due to the high electrode–electrolyte interface area. Galvanostatic charge–discharge tests show that NLTO exhibits a higher rate capability of 151.8 mAh g^{-1} at 10 C than that of LTO (139.1 mAh g^{-1} at 10 C), suggesting that N-doping is beneficial to the improvement in high-rate capability of the $Li_4Ti_5O_{12}$ nanosheets.

1. Introduction

With growing concerns over the global warming effect coming from the production of carbon dioxide and the energy crisis of fossil fuels, developing new power sources for renewable energy systems and next-generation vehicles such as electric vehicles (EVs) and hybrid electric vehicles (HEVs) to save oil and to decrease exhaust emissions are very significant [1]. Lithium ion batteries (LIBs) with the highest energy density and power are believed to be the most suitable energy storage device for those applications [2]. One of the key safety issues in LIBs for HEVs would be the dendritic lithium growth on the anode surface at high charging current because the conventional carbonous materials approach almost 0 V versus Li/Li^+ at the end of Li insertion [3].

As an alternative anode material to carbon, spinel lithium titanate ($Li_4Ti_5O_{12}$) has been intensively investigated for lithium-ion batteries owing to its high redox potential (~1.55 V, vs. Li/Li^+), excellent reversibility, high structural and thermodynamic stability [4–6]. Nevertheless, a main obstacle that impedes the widespread applications of $Li_4Ti_5O_{12}$ is its poor conductivity associated with poor charge/discharge properties at high rates [7]. Several methods have been used to increase electronic conductivity with the intent of improving rate capability, including forming a composite of $Li_4Ti_5O_{12}$ and conductive phase [8–12], doping $Li_4Ti_5O_{12}$ with metal ions [13–18] or non-metal ions [19,20]. Doping with Nitrogen has been proved to be a practical method to improve the rate capability of $Li_4Ti_5O_{12}$ [21,22]. For example, Shao et al. [21] fabricated nitrogen/TiN modified LTO with enhanced rate performance by applying ammonia as the atmosphere during solid-state reaction at 800 °C. Compared with micro-sized LTO particles, nanosheets structure

* Corresponding authors. Tel./fax: +86 21 35303544.
E-mail addresses: wangbaofeng@shiep.edu.cn, boldwinwang@gmail.com (B. Wang), tangyufeng@mail.sic.ac.cn (Y. Tang).

http://dx.doi.org/10.1016/j.jpowsour.2014.05.009
0378-7753/

enable facile charge transfer reactions and short Li^+ diffusion paths. Taking the advantages of N-doping and nanosheets structure, a higher-performance electrode material is expected to be achieved. However, research works based on N-doping LTO-nanosheets have been rarely tackled. For fabricating well-crystallized doped-LTO, a high calcining temperature (typically >700 °C) is needed [13–21]. Nonetheless, it is not feasible to fabricate nanostructured LTO. This is because nano $Li_4Ti_5O_{12}$ will seriously aggregate and lose their nano-structure at such high temperature, which will prolong Li^+ diffusion paths and worsen the electrochemical performance of LTO.

Herein, we report on the preparation of N-doped $Li_4Ti_5O_{12}$ nanosheets for high-rate lithium ion batteries via a hydrothermal reaction with further heat-treatment at low temperature. The hydrous lithium titanate (LHTO) nanosheets are synthesized through a simple hydrothermal reaction method [23], and then the as-synthesized LHTO nanosheets can be crystallized and doped under NH_3 atmosphere at a low calcination temperature of ca. 500 °C. The resulting N-doped $Li_4Ti_5O_{12}$ nanosheets have a capacity of 151.8 mAh g^{-1} at 10 C-rate.

2. Experimental

2.1. Preparation of pristine $Li_4Ti_5O_{12}$ (LTO) and N-doped $Li_4Ti_5O_{12}$ (NLTO)

In a typical procedure, 4 mmol TiO_2 colloids, obtained from the hydrolysis of 1.4 mL tetrabutyl titanate in ethanol/water mixed solution, was mixed with 20 mL 0.2 mol L^{-1} LiOH solution in a teflon-lined stainless autoclave, which was maintained at 150 °C for 14 h and then cooled to room temperature naturally. The resulting white precipitate was recovered by centrifugation, washed with deionized water and ethanol thoroughly, and then dried in an oven at 80 °C. Finally, the as-prepared sample was calcinated in a tube furnace at 500 °C for 6 h in air atmosphere to obtain LTO and in NH_3 atmosphere to obtain NLTO.

2.2. Physical characterization

The materials were characterized by X-ray diffraction measurement (XRD, Rigaku D/max-RB using Cu Kα radiation), transmission electron microscopy (TEM, JEOL 2100F), field emitting scanning electron microscopy (FE-SEM, Hitachi S-4800) equipped with an energy dispersive spectroscope (EDS) and inductively coupled plasma emission spectroscopy (ICP, Shimadzu ICPS-7510). X-ray photoelectron spectroscopy (XPS) measurements were carried out by a Kratos Axis UltraDLD spectrometer (Kratos Analytical-A Shimadzu group company) using a monochromatic Al Kα radiation ($h\gamma$ = 1486.6 eV). The binding energies of the samples were calibrated by taking the carbon 1 s peak as a reference (284.6 eV).

2.3. Electrochemical tests

Electrochemical experiments were carried out via CR2016 coin-type test cells assembled in an argon-filled glove box using lithium metal as counter electrodes. The composite electrodes were made of the active materials powder (80 wt%), acetylene black (10 wt%) and polyvinylidene fluoride (PVDF) binder (10 wt%) homogeneously mixed in N-methyl pyrrolidinone (NMP) solvent and then coated uniformly on a copper foil. Disks of 1.54 cm^2 were punched out of the foil, and the weight of the active material for each disk was about 3.5 mg. The electrolyte consisted of a solution of 1 M $LiPF_6$ in ethylene carbonate (EC), dimethyl carbonate (DMC) and ethyl methyl carbonate (EMC) solution (1:1:1 in volume). The discharge–charge measurements were performed on Land CT2001A tester (Wuhan, China) at the constant current mode in the range of 1.0–2.5 V. The cyclic voltammetry was tested at a scan rate of 0.1 mV s^{-1} using Autolab PGSTAT 302N electrochemical workstation, between 1.0 and 2.5 V. The electrochemical impedance of the electrode was studied in a three-electrode glass cell with metallic lithium film as both counter and reference electrodes. The experiment was performed using Autolab PGSTAT 302N electrochemical workstation in a frequency range of 100 kHz–0.1 Hz and a potentiostatic signal amplitude of 5 mV at full charge state (2.5 V). Prior to the EIS measurements, the electrode was activated by three cycles charge/discharge at 0.2 C between 1.0 V and 2.5 V.

3. Results and discussion

The XRD patterns of the as prepared LHTO, LTO and NLTO are shown in Fig. 1. The diffraction peaks of as synthesized LHTO (Fig. 1a) can be indexed as the layered hydrous lithium titanate with a C-base-centered orthorhombic lattice (JCPDS No. 47-0123). As the results previously reported, such layered hydrothermal products can be transformed to spinel $Li_4Ti_5O_{12}$ after heat treatment [23]. From Fig. 1b and c, we can see all the peaks are in accordance with the standard diffraction peaks of cubic spinel $Li_4Ti_5O_{12}$ (JCPDS No. 49-0207) and no characteristic peaks are observed for other impurities in both LTO and NLTO. These results reveal that the LHTO can be completely converted to cubic spinel LTO after heat-treatment at 500 °C for 6 h in both air and NH_3 atmosphere. There is no distinct difference between the patterns of LTO (Fig. 1b) and NLTO (Fig. 1c), indicating that the N-doping has not changed the crystal structure of $Li_4Ti_5O_{12}$. But the obvious difference is that the white LTO becomes brown after N-doping as shown in the inset of Fig. 1. The change of color can be ascribed to partial reduction of Ti^{4+} on the LTO surface to Ti^{3+}. Moreover, the lattice parameter of LTO and NLTO obtained by analyzing XRD pattern is estimated to be 8.353 Å and 8.347 Å, respectively. A slight change of lattice parameter occurred due to the doping of N at a low annealing temperature.

The chemical information of the product was examined by XPS and shown in Fig. 2. The wide-survey XPS spectrum (Fig. 2a) of the as-synthesized NLTO reveals the main presence of Ti, O and C in the NLTO. Additionally, in the XPS spectrum (Fig. 2b), a pronounced nitrogen peak at 396 eV can be seen, which is assigned to N in covalent Ti–N bonds [24]. The peak of N1s appeared in the XPS indicates that the LTO surface is doped with nitrogen. The high

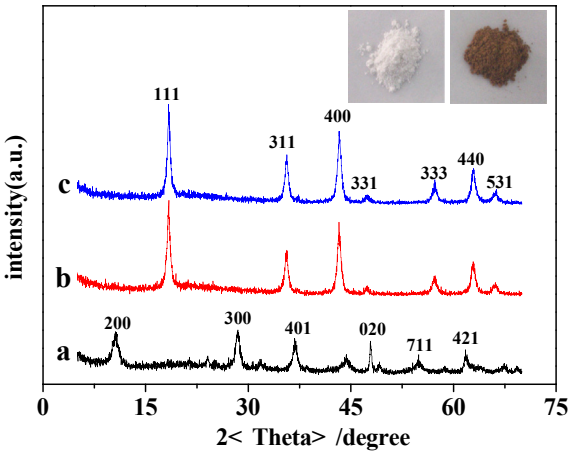

Fig. 1. X-ray diffraction patterns of (a) LHTO, (b) LTO, (c) NLTO, and inset is the photograph of the LTO (left) and NLTO (right) with white color and brown color, respectively. (For interpretation of the references to color in this figure legend, the reader is referred to the web version of this article.)

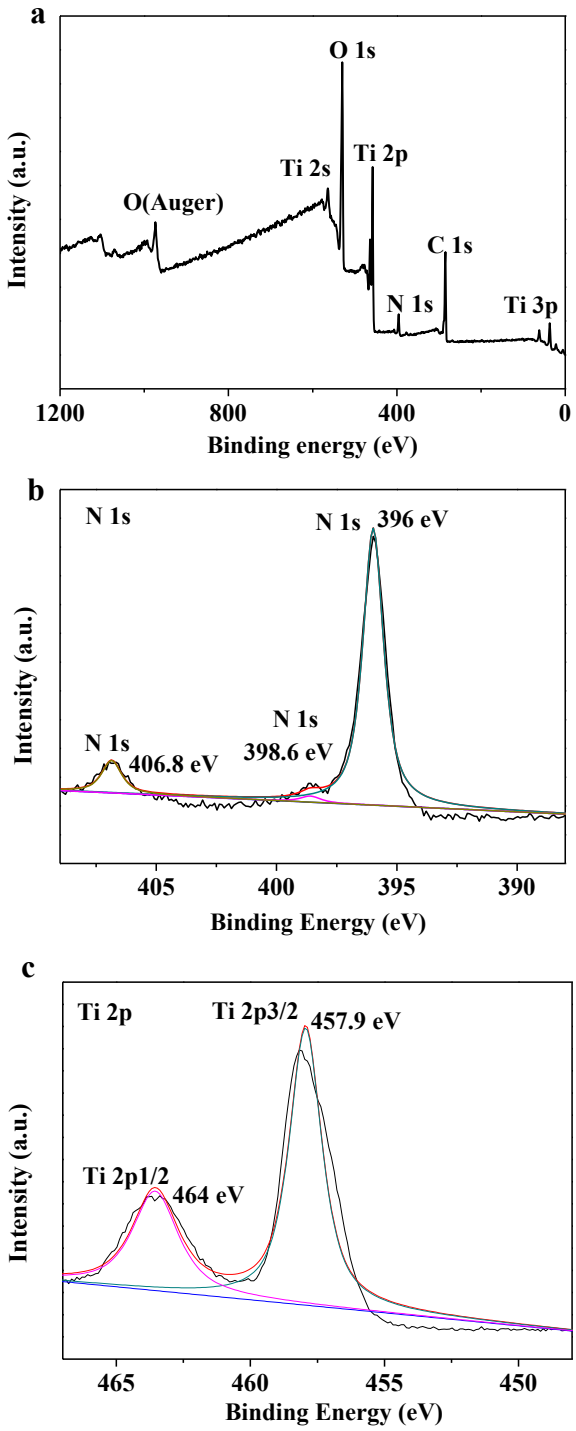

Fig. 2. (a) The wide-survey XPS spectrum of NLTO; (b) N 1s XPS spectrum; (c) Ti 2p XPS spectrum.

resolution spectra of the Ti 2p are shown in Fig. 2c. It can be seen that Ti 2p spectra consists of two peaks at around 457.9 eV (Ti 2p3/2) and 464.2 eV (Ti 2p1/2). According to previous studies [25,26], the Ti 2p3/2 peak of Ti_2O_3 is located at 458.0 eV. Accordingly, the shift of Ti 2p3/2 of NLTO to 457.9 eV represents a state close to Ti^{3+}, suggesting a mixed Ti^{4+}/Ti^{3+} valence of Ti ions. After calcining in ammonia atmosphere, LHTO transforms to LTO along with the partial reduction of Ti^{4+} on the LTO surface to Ti^{3+}, which would lead to electrons' increase and eventually improve electronic conductivity.

SEM and TEM were applied to investigate the effect of N-doping on morphology. As shown in Fig. 3a and c, the morphology of both NLTO and LTO can be described as nanosheets with very similar irregular shape, indicating that N-doping under a low calcination temperature almost has no obvious effect on the morphology of the materials. The nanosheets structure can not only shorten the electronic path, but also facile transport of the electrolyte to the surfaces of the LTO, thus results in rapid charge transfer and short Li^+ diffusion distance. TEM images of LTO and NLTO are shown in Fig. 3b and d. The images clearly reveal that the sample is composed of stacked nanosheets. Lattice fringes can be seen clearly (Fig. 3d), suggesting that these sheets have a well-defined cubic crystalline structure. The peak of N in EDS corroborates that NLTO powders indeed contain the N element, which corresponds with the result of XPS. The EDS analyses show that the atomic percentage of Ti, O and N is 28.08%, 70.15% and 1.77% respectively. The ICP results also indicate that the mole ratio of Li: Ti is 0.78, which is close to that in $Li_4Ti_5O_{12}$.

The electrochemical performance of NLTO microspheres was systematically investigated using a coin-type half cell. Cyclic voltammograms (CVs) curves of LTO and NLTO are shown in Fig. 4a. It can be seen from Fig. 4a that there is a pair of similar reversible redox peaks for LTO and NLTO, suggesting that N-doping do not change the electrochemical reaction process of LTO. The anodic peaks at about 1.70 V (vs. Li/Li^+) and the cathodic peaks at around 1.45 V (vs. Li/Li^+) are correspond to the processes of Li deintercalation and intercalation. The voltage differences between anodic and cathodic peaks reflect the polarization degree of the electrode. Compared to the LTO, the cathodic and anodic peaks of the NLTO are much higher and sharper, which indicates the better electrode kinetic of the NLTO. In addition, the potential difference between cathodic and anodic peaks of the NLTO (0.15 V) is smaller than that of the LTO (0.25 V), which suggests that N-doping is favorable for reducing the electrode polarization.

Fig. 4b shows the initial charge/discharge profiles of the LTO and NLTO at 1 C rate. The C rates are calculated based on 1 C = 175 mA g^{-1}. Both electrodes present voltage plateau around 1.55 V, which are the result of a two-phase reaction based on the redox couple of Ti^{3+}/Ti^{4+}. However, the NLTO presents a more flat plateau profile and a larger plateau capacity than the LTO, and the polarization between the charge and discharge plateau is 160 mV for LTO and only 52 mV for NLTO, indicating that the kinetics of the pristine LTO are indeed improved after N-doping. The reason can be explained associated with the presence of the Ti^{3+}, which has been considered to be helpful to the improvement in electrochemical performance [27].

Fig. 4c compares the rate capabilities of pristine LTO and NLTO electrodes. For each stage, the charge–discharge processes of the samples are taken for 20 cycles. As shown in Fig. 4c, the NLTO electrode delivered a capacity of 173.3, 165.1, 162.3 and 151.8 mAh g^{-1} at 1, 2, 5 and 10 C, respectively. As for LTO electrode, the capacity is 170.6, 163, 156.9 and 139.1 mAh g^{-1}, respectively. Therefore, NLTO exhibits obviously improved capacity. Moreover, as the current rate returned to 1 C again, a stable capacity of 172.6 mAh g^{-1} can be obtained with rare decaying in the following 20 cycles, demonstrating that the NLTO electrode has an excellent reversibility and stability. The significant improvement in high rate performance of the NLTO is attributed to the Ti^{3+} that improves the electrochemical activity of the composite [27].

The NLTO sample is further subjected to cycling performance evolution at 1 C and 10 C rate, shown in Fig. 4d. At 1 C, NLTO cell reaches a reversible capacity of 165.3 mAh g^{-1} after 200 cycles, which keeps 95.8% of its initial discharge capacity (172.5 mAh g^{-1}). Furthermore, a discharge capacity of 144 mAh g^{-1} after 200 cycles is still achieved at 10 C rate. The superior cycling stability is attributed to the combinative advantages of nanosheets structure

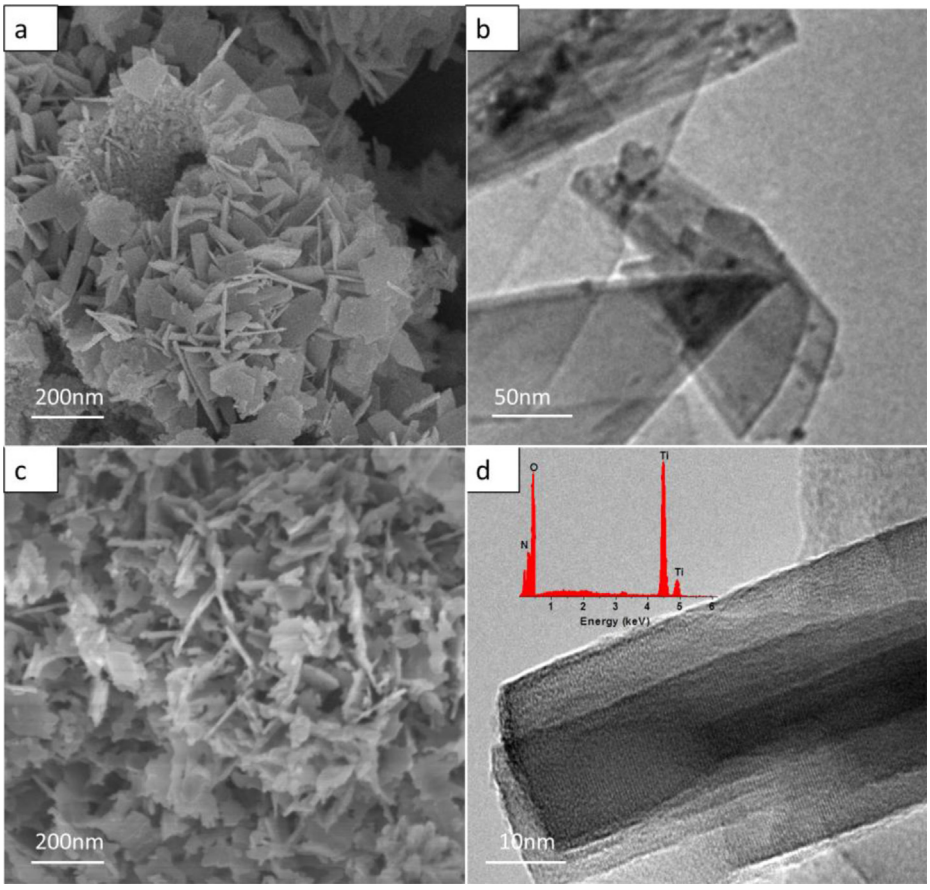

Fig. 3. SEM images of LTO (a) and NLTO (c), TEM images of LTO (b) and NLTO (d) (inset shows the EDS result).

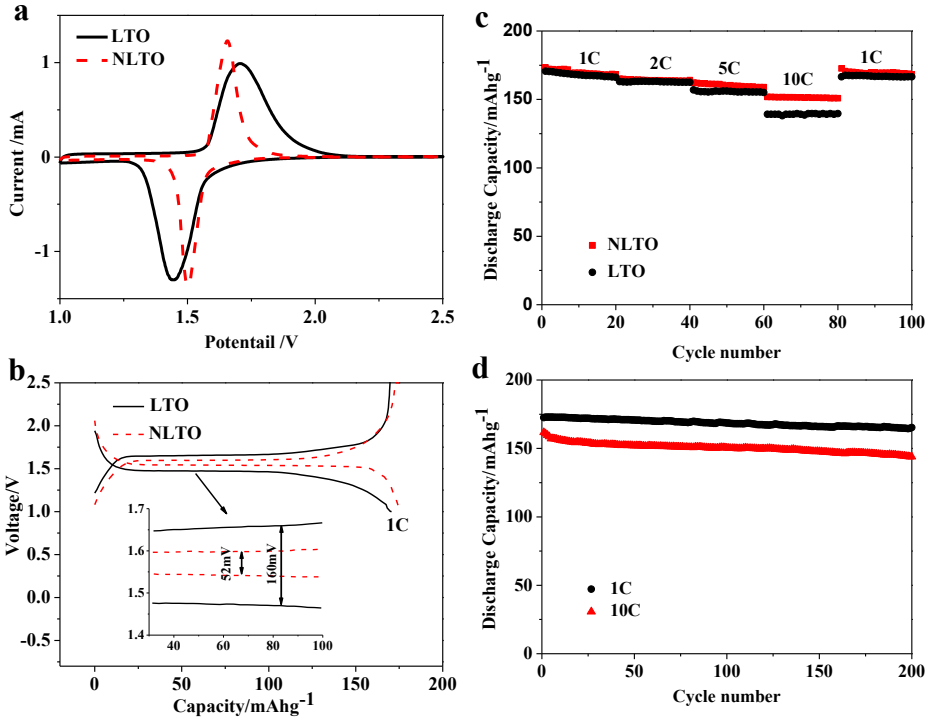

Fig. 4. (a) Cyclic voltammograms (CVs) of LTO and NLTO electrodes at a scan rate of 0.1 mV s^{-1}, (b) the first charge/discharge profiles of the LTO and NLTO at 1 C rate, the inset shows the magnified region, (c) comparison of the rate capabilities of LTO and NLTO electrodes, (d) cycle performance of NLTO electrodes at 1 C and 10 C rate.

and N-doping modification. On the one hand, the nanosheets structure can shorten the ion and electron transfer path and increase electrode/electrolyte contact area. On the other hand, N-doping modification can enhance the conductivity of LTO due to the presence of Ti^{3+} valence on surface.

Fig. 5a shows EIS curves of LTO and NLTO electrodes tested in three electrodes system. An equivalent circuit used to fit the spectra is given in the inset of Fig. 5a. For both LTO and NLTO electrodes, a semicircle in high frequency region and a line in low frequency region were observed. Rs represents the electrolyte resistance; CPE and Rct represent constant phase element and charge transfer resistance, respectively. The charge transfer resistance can be calculated according to the depressed semicircle; Zw represents Warburg impedance. It can be clearly seen from Fig. 5a that NLTO electrodes have a smaller charge-transfer resistance than that of LTO electrodes, indicating that the N-doped LTO possesses higher conductivity. The lithium ion diffusion coefficient can be calculated from the formula as following equation [28,29]:

$$D = R^2T^2 \Big/ 2A^2n^4C^2\sigma^2$$

where R is the gas constant, T is the absolute temperature, n is the number of electrons transferred per molecule during oxidization, F is the Faraday constant, A is the surface area of the electrode, C is the concentration of Li ions and σ is the slope of the line $Z' \sim \omega^{-1/2}$, which can be obtained from the line of $Z' \sim \omega^{-1/2}$ (shown in Fig. 5b).

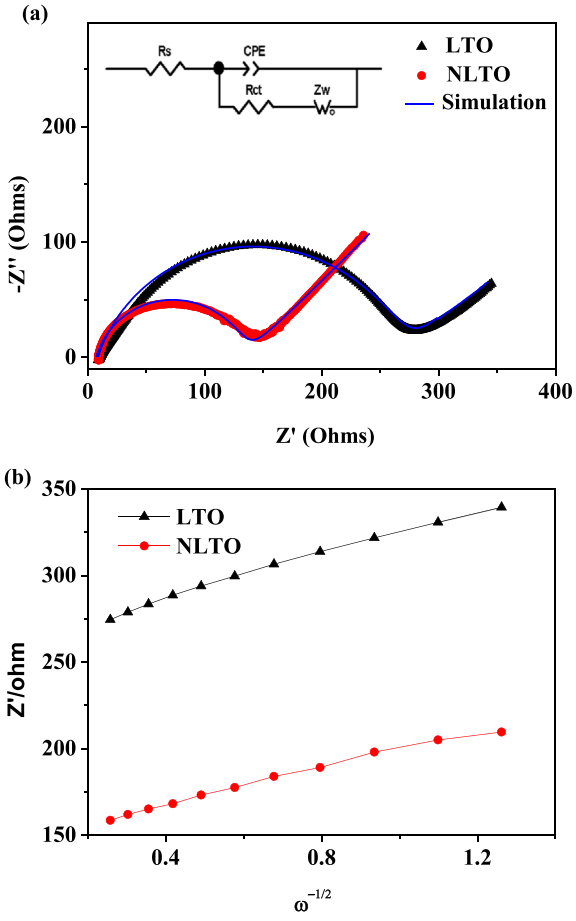

Fig. 5. (a) Impedance spectra of LTO and NLTO electrodes within frequency range of 100 kHz–0.1 Hz. The inset is the equivalent circuit used to fit the EIS. (b) Graph of Z' plotted against $\omega^{-1/2}$ at low frequency region (2.4–0.1 Hz) for LTO and NLTO electrodes.

The calculated lithium diffusion coefficient D ($cm^2\ s^{-1}$) of NLTO material is 1.56×10^{-14} $cm^2\ s^{-1}$, however that of LTO is only 4.64×10^{-15} $cm^2\ s^{-1}$. Obviously, the NLTO has a bigger lithium ion diffusion coefficient, which indicates that the lithium-ion mobility of $Li_4Ti_5O_{12}$ can be effectively improved by N doping. Consequently, the electrochemical performance of $Li_4Ti_5O_{12}$ can be improved effectively.

4. Conclusions

Nitrogen-doped $Li_4Ti_5O_{12}$ nanosheets were successfully prepared via a hydrothermal process and following low temperature sintering in NH_3 atmosphere. XPS, EDS and XRD results show the presence of Ti^{3+} on LTO surface after N-doping. The Ti^{3+} is beneficial to improve the conductivity of the composite. When used as anode, NLTO shows a better rate capability and Cycle stability. After 200 cycles, its discharge capacity is 144 mAh g^{-1} at 10 C. The excellent rate capability can be attributed to the enhanced conductivity of the N-doping modification combined with the short ion and electron transfer paths of nanosheet structures. Such results indicate that the N-doped $Li_4Ti_5O_{12}$ nanosheets can be attractive candidate anode materials for lithium ion batteries.

Acknowledgments

This work has been carried out with the financial support of Shanghai Municipal Education Commission, China ("085" program).

References

[1] J.B. Goodenough, Y. Kim, Chem. Mater. 22 (2010) 587–603.
[2] M. Armand, J.M. Tarascon, Nature 451 (2008) 652–657.
[3] S.S. Zhang, J. Power Sources 161 (2006) 1385–1391.
[4] L. Cheng, J. Yan, G.N. Zhu, J.Y. Luo, C.X. Wang, Y.Y. Xia, J. Mater. Chem. 20 (2010) 595–602.
[5] T.F. Yi, Y. Xie, Y.R. Zhu, R.S. Zhu, H.Y. Shen, J. Power Sources 222 (2013) 448–454.
[6] T. Doi, Y. Miwa, Y. Iriyama, T. Abe, Z. Ogumi, J. Phys. Chem. C 113 (2009) 7719–7722.
[7] J. Huang, Z. Jiang, Electrochim. Acta 53 (2008) 7756–7759.
[8] W. Fang, X.Q. Cheng, P.J. Zuo, Y.L. Ma, G.P. Yin, Electrochim. Acta 93 (2013) 173–178.
[9] Y.Q. Wang, L. Gu, Y.G. Guo, H. Li, X.Q. He, S. Tsukimoto, Y. Ikuhara, L.J. Wan, J. Am. Chem. Soc. 134 (2012) 7874–7879.
[10] S.G. Ria, L. Zhan, Y. Wang, L.H. Zhou, J. Hua, H.L. Liu, Electrochim. Acta 109 (2013) 389–394.
[11] G.W. Xie, J.F. Ni, X.F. Liao, L.J. Gao, Mater. Lett. 78 (2012) 177–179.
[12] H.F. Ni, L.Z. Fan, J. Power Sources 214 (2012) 195–199.
[13] T.F. Yi, S.Y. Yang, X.Y. Li, J.H. Yao, Y.R. Zhu, R.S. Zhu, J. Power Sources 246 (2014) 505–511.
[14] T.F. Yi, H.P. Liu, Y.R. Zhu, L.J. Jiang, Y. Xie, R.S. Zhu, J. Power Sources 215 (2012) 258–265.
[15] C.X. Qiu, Z.Z. Yuan, L. Liu, N. Ye, J.C. Liu, J. Solid State Electrochem. 17 (2013) 841–847.
[16] T.F. Yi, B. Chen, H.Y. Shen, R.S. Zhu, A.N. Zhou, H.B. Qiao, J. Alloy. Compd. 558 (2013) 11–17.
[17] B.B. Tian, H.F. Xiang, L. Zhang, H.H. Wang, J. Solid State Electrochem. 16 (2012) 205–211.
[18] Q.Y. Zhang, C.L. Zhang, B. Li, D.D. Jiang, S.F. Kang, Xi Li, Y.G. Wang, Electrochim. Acta 107 (2013) 139–146.
[19] Y.S. Hu, L. Kienle, Y.G. Guo, J. Maier, Adv. Mater. 18 (2006) 1421–1426.
[20] Y. Qi, Y. Huang, D. Jia, S.J. Bao, Z.P. Guo, Electrochim. Acta 54 (2009) 4772–4776.
[21] Z.N. Wan, R. Cai, S.M. Jiang, Z.P. Shao, J. Mater. Chem. 22 (2012) 17773–17781.
[22] K.S. Park, A. Benayad, D.J. Kang, S.G. Doo, J. Am. Chem. Soc. 130 (2008) 14930–14931.
[23] J.Z. Chen, L. Yang, S.H. Fang, Y.F. Tang, Electrochim. Acta 55 (2010) 6596–6600.
[24] J. Wang, D.N. Tafen, J.P. Lewis, Z. Hong, A. Manivannan, M. Zhi, M. Li, N. Wu, J. Am. Chem. Soc. 131 (2009) 12290–12297.
[25] F. Werfel, O. Brümmer, Phys. Scr. 28 (1983) 92.
[26] Y. Chen, X. Cao, B. Lin, B. Gao, Appl. Surf. Sci. 264 (2013) 845–852.
[27] J. Wolfenstine, U. Lee, J.L. Allen, J. Power Sources 154 (2006) 287–289.
[28] Y.J. Gu, Z. Guo, H.Q. Liu, Electrochim. Acta 123 (2014) 576–581.
[29] X.Y. Wang, H. Hao, J.L. Liu, T. Huang, A.S. Yu, Electrochim. Acta 56 (2011) 4065–4069.